

Novel Schiff base ligand and its metal complexes with some transition elements. Synthesis, spectroscopic, thermal analysis, antimicrobial and *in vitro* anticancer activity

Walaa H. Mahmoud*, Reem G. Deghadi and Gehad G. Mohamed



A novel Schiff base ligand (H_2L) was prepared through condensation of 2,6-diaminopyridine and *o*-benzoylbenzoic acid in a 1:2 ratio. This Schiff base ligand was characterized using elemental and spectroscopic analyses. A new series of Cr(III), Mn(II), Fe(III), Co(II), Ni(II), Cu(II), Zn(II) and Cd(II) metal complexes of H_2L were prepared and characterized using elemental analysis, spectroscopy (1H NMR, mass, UV-visible, Fourier transform infrared, electron spin resonance), magnetic susceptibility, molar conductivity, X-ray powder diffraction and thermal analysis. The complexes are found to have trigonal bipyramidal geometry except Cr(III), Mn(II) and Fe(III) complexes which have octahedral geometry based on magnetic moment and solid reflectance measurements. The infrared spectral studies reveal that H_2L behaves as a neutral bidentate ligand and coordinates to the metal ions via the two azomethine nitrogens. 1H NMR spectra confirm the non-involvement of the carboxylic COOH proton in complex formation. The presence of water molecules in all reported complexes is supported by thermogravimetric studies. Kinetic and thermodynamic parameters were determined using Coats-Redfern and Horowitz-Metzger equations. The synthesized ligand and its complexes were screened for antimicrobial activities against two Gram-positive bacteria (*Bacillus subtilis* and *Staphylococcus aureus*), two Gram-negative bacteria (*Escherichia coli* and *Neisseria gonorrhoeae*) and one fungus (*Candida albicans*). Anticancer activities of the ligand and its metal complexes against human breast cancer cell line (MCF7) were investigated. Copyright © 2016 John Wiley & Sons, Ltd.

Additional supporting information may be found in the online version of this article at the publisher's web site.

Keywords: Schiff base ligand; spectroscopic analyses; thermal analysis; kinetic; antimicrobial activities; breast cancer

Introduction

For decades, coordination chemistry of Schiff base ligands has been the subject of great interest. Schiff bases are capable of forming coordinate bonds with many metal ions via azomethine and phenolic groups, so they have been used for the synthesis of metal complexes due to their easy formation and strong metal binding ability.^[1]

A broad variety of Schiff base ligands and their complexes can be utilized for metal biosite modelling, models of reaction centres of metalloenzymes, nonlinear optical materials, catalysts for many organic reactions, effective catalysts in asymmetric synthesis and luminescence materials.^[2,3] Furthermore these compounds exhibit biological activity as anticancer, antifungal, antibacterial, antiviral and antiparasitic agents in addition to other biological performances. These compounds have also played a great role in the development of chemistry.^[4-6]

The structure of 2,6-diaminopyridine has a symmetrical feature, possessing three nitrogen lone pairs. Pyridine is one of the most common heterocyclic compounds found in various therapeutic agents.^[7] Pyridine-based Schiff base systems are important in metal chelation, host-guest systems, extraction, enzyme mimics, antibiotics and natural products such as marine alkaloids.^[8] Some Schiff bases can be derived from condensation of 2,6-

diaminopyridine with other compounds such as 1,4-bis(2-carboxyaldehydephenoxy)butane,^[9] 1,7-bis(2-formylphenyl)-1,4,7-trioxahexane,^[10] 1,3-bis(2-carboxyaldehydephenoxy)propane^[11] and 1,2-bis(2-carboxyaldehydephenoxy)ethane.^[12]

In the work presented here, a new Schiff base ligand was synthesized by condensation of 2,6-diaminopyridine with *o*-benzoylbenzoic acid. Its coordination behaviour with various transition metal ions was studied. The anticancer and antimicrobial activities are also discussed.

Experimental

Materials and reagents

All chemicals used were of analytical reagent grade (AR), and of highest purity available. They included 2,6-diaminopyridine (Acros), *o*-benzoylbenzoic acid (Sigma), $CrCl_3 \cdot 6H_2O$ (Sigma), $MnCl_2 \cdot 2H_2O$ (Sigma), $NiCl_2 \cdot 6H_2O$ (BDH), $FeCl_3 \cdot 6H_2O$ (Prolabo), $CoCl_2 \cdot 6H_2O$

* Correspondence to: Walaa H. Mahmoud, Chemistry Department, Faculty of Science, Cairo University, Giza 12613, Egypt. E-mail: dr.walaa@yahoo.com

Chemistry Department, Faculty of Science, Cairo University, Giza 12613, Egypt

(Aldrich), $\text{CuCl}_2 \cdot 2\text{H}_2\text{O}$ (Merck), CdCl_2 (Aldrich) and ZnCl_2 (Strem Chemicals). Dimethylsulfoxide (DMSO), RPMI-1640 medium, sodium bicarbonate, isotonic trypan blue, foetal bovine serum (FBS), penicillin, streptomycin, trypsin, acetic acid, sulforhodamine-B (SRB) and trichloroacetic acid were supplied by Sigma Chemical Co., St Louis, MO, USA. Organic solvents used were ethyl alcohol (90%) and dimethylformamide (DMF). Deionized water was usually used in all preparations.

Solutions

Stock solutions of metal complexes at a concentration of 1×10^{-3} M were prepared by dissolving a certain weight in DMF for measuring the conductivity for all metal complexes. Solutions of the Schiff base ligand and its metal complexes (1×10^{-4} M), except for Cu(II) and Fe(III) (5×10^{-5} M), were prepared by dilution of the previously prepared solutions to measure UV-visible spectra.

Anticancer activity experiments

A fresh stock solution (1×10^{-3} M) of Schiff base ligand (0.0012 g L^{-1}) was prepared in the appropriate volume of ethanol (90%). DMSO was used in cryopreservation of cells. RPMI-1640 medium was used. The medium was used for culturing and maintenance of the human tumour cell line. The medium was supplied in a powder form. It was prepared as follows: 10.4 g of medium was weighed, mixed with 2 g of sodium bicarbonate, completed to 1 L with distilled water and shaken carefully until complete dissolution. The medium was then sterilized by filtration in a Millipore bacterial filter (0.22 mL). The prepared medium was kept in a refrigerator (4°C) and checked at regular intervals for contamination. Before use, the medium was warmed at 37°C in a water bath and supplemented with penicillin–streptomycin and FBS. Sodium bicarbonate was used for the preparation of RPMI-1640 medium. Isotonic trypan blue solution (0.05%) was prepared in normal saline and was used for viability counting. FBS (10%, heat inactivated at 56°C for 30 min), 100 units mL^{-1} penicillin and 2 mg mL^{-1} streptomycin were used for the supplementation of RPMI-1640 medium prior to use. Trypsin (0.025% w/v) was used for the harvesting of cells. Acetic acid (1% v/v) was used for dissolving unbound SRB dye. SRB (0.4%) dissolved in 1% acetic acid was used as a protein dye. A stock solution of trichloroacetic acid (50%) was prepared and stored. An amount of 50 μL of the stock was added to 200 μL of RPMI-1640 medium per well to yield a final concentration of 10% used for protein precipitation. Isopropanol (100%) and ethanol (70%) were used. Tris base (10 mM; pH = 10.5) was used for SRB dye solubilization. Tris base (121.1 g) was dissolved in 1000 mL of distilled water and the pH was adjusted using hydrochloric acid (2 M).

Instrumentation

Microanalyses of carbon, hydrogen and nitrogen were carried out at the Microanalytical Center, Cairo University, Egypt, using a CHNS-932 (LECO) Vario elemental analyser. Analyses of the metals were conducted by dissolving the solid complexes in concentrated HNO_3 , neutralizing the diluted aqueous solutions with ammonia and titrating the metal solutions with EDTA.

Fourier transform infrared (FT-IR) spectra were recorded with a PerkinElmer 1650 spectrometer ($400\text{--}4000 \text{ cm}^{-1}$) in KBr pellets.

Electronic spectra were recorded at room temperature as solutions in ethanol with a Shimadzu 3101pc spectrophotometer. ^1H NMR spectra, as solutions in $\text{DMSO-}d_6$, were recorded with a 300 MHz Varian-Oxford Mercury at room temperature using tetramethylsilane as an internal standard. Electron spin resonance spectra were recorded with a JES-FE2XG ESR spectrophotometer at the Microanalytical Center, Tanta University. Mass spectra were recorded using the electron ionization technique at 70 eV with an MS-5988 GS-MS Hewlett-Packard instrument at the Microanalytical Center, National Center for Research, Egypt. UV-visible spectra were obtained with a Shimadzu UVmini-1240 spectrophotometer.

Molar magnetic susceptibility was measured on powdered samples using the Faraday method. Diamagnetic corrections were made using Pascal's constant and $\text{Hg}[\text{Co}(\text{SCN})_4]$ was used as a calibrant. Molar conductivities of 10^{-3} M solutions of the solid complexes in ethanol were measured using a Jenway 4010 conductivity meter.

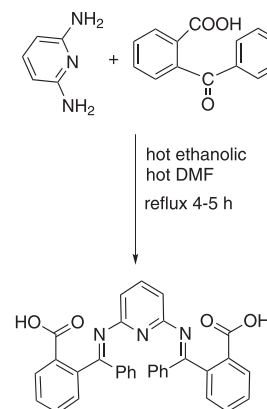
Thermogravimetric (TG) and differential thermogravimetric (DTG) analyses of the solid complexes were carried out from room temperature to 1000°C using a Shimadzu TG-50H thermal analyser.

Powder X-ray diffraction (XRD) analyses were carried out using a Philips Analytical X-ray diffractometer, type PW 1840. Radiation was provided by a copper target (Cu anode, 2000 W) high-intensity X-ray tube operated at 40 kV and 25 mA. Divergence and the receiving slits were 1 and 0.2, respectively.

Antimicrobial measurements were carried out at the Microanalytical Center, Cairo University, Egypt. Anticancer activity experiments were performed at the National Cancer Institute, Cancer Biology Department, Pharmacology Department, Cairo University. The optical density (OD) of each well was measured spectrophotometrically at 564 nm with an ELIZA microplate reader (Meter tech. R 960, USA).

Synthesis of Schiff base ligand

The symmetric Schiff base ligand (H_2L) was synthesized by condensation of 2,6-diaminopyridine with *o*-benzoylbenzoic acid (1). A solution of *o*-benzoylbenzoic acid (55 mmol, 12.4 g) dissolved in DMF was added dropwise to 2,6-diaminopyridine (27.5 mmol, 3 g) dissolved in ethanol. The resulting mixture was stirred under reflux for about 4–5 h at $100\text{--}150^\circ\text{C}$, during which a yellowish green solid compound was separated. It was filtered, washed, recrystallized from diethyl ether and dried in vacuum.



Scheme 1. Synthesis of symmetric Schiff base ligand (H_2L).

Yield 90%; m.p. 130°C; yellowish green solid. Anal. Calcd for $C_{33}H_{23}N_3O_4$ (%): C, 75.43; H, 4.38; N, 8.0. Found (%): C, 75.40; H, 4.46; N, 7.74. FT-IR (cm^{-1}): hydroxyl $\nu(OH)$ 3455, azomethine $\nu(C=N)$ 1596, asymmetric carboxylic $\nu(COO^-)_{asym}$ 1540, symmetric carboxylic $\nu(COO^-)_{sym}$ 1380. 1H NMR (300 MHz, DMSO- d_6 , δ , ppm): 7.17–8.00 (m, 21H, Ar H), 5.68 (s, 2H, OH carboxylate). ^{13}C NMR (300 MHz, DMSO- d_6 , δ , ppm): 161.6 (C1 and C6; pyridine ring), 114.3 (C2 and C4; pyridine ring), 136.5 (C3; pyridine ring), 174.1 (C5; C=N azomethine), 167.5 (C14; COOH), 136.4 (C6; Ar), 129 (C7, C11; Ar), 128.6 (C8, C10; Ar), 130.8 (C9, Ar), 137.7 (C12; benzoic), 131.6 (C13; benzoic), 128.3 (C15; benzoic), 130.6 (C16; benzoic), 133.8 (C17; benzoic), 125.8 (C18; benzoic). λ_{max} (nm): 217 and 246 $\pi-\pi^*$, 333 $n-\pi^*$.

Synthesis of metal complexes

Complexes of H_2L with Cr(III), Mn(II), Fe(III), Co(II), Ni(II), Cu(II), Zn(II) and Cd(II) metal ions were prepared by reaction of 1:1 molar mixture of hot ethanolic solution (60°C) of the appropriate metal chloride (0.76 mmol) and H_2L (0.4 g, 0.76 mmol). The resulting mixture was stirred under reflux for 1 h whereupon the complexes precipitated. They were collected by filtration and purified by washing several times with diethyl ether.

CrH₂L

Yield 88%; green solid, m.p. 118°C. Anal. Calcd for $Cr(C_{33}H_{31}Cl_3N_3O_8)$ (%): C, 52.42; H, 4.10; N, 5.56; Cr, 6.88. Found (%): C, 52.10; H, 4.50; N, 5.70; Cr, 6.53. FT-IR (cm^{-1}): hydroxyl $\nu(OH)$ 3319, azomethine $\nu(C=N)$ absent, asymmetric carboxylic $\nu(COO^-)_{asym}$ 1487, symmetric carboxylic $\nu(COO^-)_{sym}$ 1410, $\nu(H_2O)$ stretching bands of coordinated water 932 and 896, $\nu(M-O)$ stretching bands of coordinated water 519, metal–nitrogen bond $\nu(M-N)$ 479. λ_{max} (nm): 213 and 245 $\pi-\pi^*$, 335 $n-\pi^*$, 17 249, 20 014, 21 457 and 22 059 cm^{-1} assignable to $^4A_{2g}(F) \rightarrow ^4T_{2g}(F)$, $^4A_{2g}(F) \rightarrow ^4T_{2g}(F)$, $^4A_{2g}(F) \rightarrow ^4T_{1g}(F)$ and $^4A_{2g}(F) \rightarrow ^4T_{1g}(P)$ transitions.

MnH₂L

Yield 87%; yellowish green solid, m.p. 90°C. Anal. Calcd for $Mn(C_{33}H_{31}Cl_2N_3O_8)$ (%): C, 54.77; H, 4.29; N, 5.81; Mn, 7.61. Found (%): C, 54.33; H, 4.60; N, 5.58; Mn, 8.01. FT-IR (cm^{-1}): hydroxyl $\nu(OH)$ 3450, azomethine $\nu(C=N)$ 1615, asymmetric carboxylic $\nu(COO^-)_{asym}$ 1542, symmetric carboxylic $\nu(COO^-)_{sym}$ 1383, $\nu(H_2O)$ stretching bands of coordinated water 931 and 837, $\nu(M-O)$ stretching bands of coordinated water 559, metal–nitrogen bond $\nu(M-N)$ 479. λ_{max} (nm): 217 and 243 $\pi-\pi^*$, 335 $n-\pi^*$, 15 560, 21 478 and 27 876 cm^{-1} assignable to $^4T_{1g} \rightarrow ^6A_{1g}$, $^4T_{2g}(G) \rightarrow ^6A_{1g}$ and $^4T_{1g}(D) \rightarrow ^6A_{1g}$ transitions.

FeH₂L

Yield 85%; black solid, m.p. 121°C. Anal. Calcd for $Fe(C_{33}H_{31}Cl_3N_3O_8)$ (%): C, 52.14; H, 4.08; N, 5.53; Fe, 7.37. Found (%): C, 51.80; H, 3.98; N, 5.84; Fe, 7.69. FT-IR (cm^{-1}): hydroxyl $\nu(OH)$ 3348, azomethine $\nu(C=N)$ 1604, asymmetric carboxylic $\nu(COO^-)_{asym}$ 1486, symmetric carboxylic $\nu(COO^-)_{sym}$ 1403, $\nu(H_2O)$ stretching bands of coordinated water 932 and 875, $\nu(M-O)$ stretching bands of coordinated water 583, metal–nitrogen bond $\nu(M-N)$ 488. λ_{max} (nm): 227 $\pi-\pi^*$, 317 $n-\pi^*$, 21 357 ($^6A_{1g} \rightarrow T_{2g}$) (G), 17 135 and 12 970 cm^{-1} ($^6A_{1g} \rightarrow ^5T_{1g}$), 24 805 cm^{-1} (ligand to metal charge transfer).

CoH₂L

Yield 89%; blue solid, m.p. 120°C. Anal. Calcd for $Co(C_{33}H_{29}Cl_2N_3O_7)$ (%): C, 55.85; H, 4.09; N, 5.92; Co, 8.32. Found (%): C, 55.84; H, 4.26; N,

6.01; Co, 8.01. FT-IR (cm^{-1}): hydroxyl $\nu(OH)$ 3415, azomethine $\nu(C=N)$ 1604, asymmetric carboxylic $\nu(COO^-)_{asym}$ 1487, symmetric carboxylic $\nu(COO^-)_{sym}$ 1389, $\nu(H_2O)$ stretching bands of coordinated water 932 and 843, $\nu(M-O)$ stretching bands of coordinated water 561, metal–nitrogen bond $\nu(M-N)$ 473. λ_{max} (nm): 213 and 245 $\pi-\pi^*$, 335 $n-\pi^*$, 13 050, 15 886 and 17 594 cm^{-1} ; fourth band at 21 378 cm^{-1} (charge transfer band).

NiH₂L

Yield 80%; yellowish green solid, m.p. 90°C. Anal. Calcd for $Ni(C_{33}H_{29}Cl_2N_3O_7)$ (%): C, 55.85; H, 4.09; N, 5.92; Ni, 8.32. Found (%): C, 56.02; H, 3.77; N, 6.23; Ni, 8.74. FT-IR (cm^{-1}): hydroxyl $\nu(OH)$ 3319, azomethine $\nu(C=N)$ 1604, asymmetric carboxylic $\nu(COO^-)_{asym}$ 1487, symmetric carboxylic $\nu(COO^-)_{sym}$ 1393, $\nu(H_2O)$ stretching bands of coordinated water 993 and 884, $\nu(M-O)$ stretching bands of coordinated water 570, metal–nitrogen bond $\nu(M-N)$ 471. λ_{max} (nm): 213 and 245 $\pi-\pi^*$, 335 $n-\pi^*$, 13 670 cm^{-1} ($^3B_1 \rightarrow ^3E$), 17 245 cm^{-1} ($^3B_1 \rightarrow ^3A_2$), 21 444 cm^{-1} ($^3B_1 \rightarrow ^3E$), 27 379 cm^{-1} (ligand to metal charge transfer).

CuH₂L

Yield 81%; black solid, m.p. >300°C. Anal. Calcd for $Cu(C_{33}H_{29}Cl_2N_3O_7)$ (%): C, 55.50; H, 4.07; N, 5.89; Cu, 8.90. Found (%): C, 55.10; H, 3.97; N, 5.81; Cu, 8.74. FT-IR (cm^{-1}): hydroxyl $\nu(OH)$ 3318, azomethine $\nu(C=N)$ 1578, asymmetric carboxylic $\nu(COO^-)_{asym}$ 1466, symmetric carboxylic $\nu(COO^-)_{sym}$ 1400, $\nu(H_2O)$ stretching bands of coordinated water 932 and 886, $\nu(M-O)$ stretching bands of coordinated water 534, metal–nitrogen bond $\nu(M-N)$ 458. λ_{max} (nm): 231 $\pi-\pi^*$, 318 $n-\pi^*$, 12 466, 15 750 and 19 945 cm^{-1} ; another band at 30 452 cm^{-1} (ligand to metal charge transfer band).

ZnH₂L

Yield 79%; yellowish green solid, m.p. 129°C. Anal. Calcd for $Zn(C_{33}H_{29}Cl_2N_3O_7)$ (%): C, 55.39; H, 4.06; N, 5.87; Zn, 9.09. Found (%): C, 55.50; H, 3.80; N, 5.57; Zn, 8.91. FT-IR (cm^{-1}): hydroxyl $\nu(OH)$ 3416, azomethine $\nu(C=N)$ 1604, asymmetric carboxylic $\nu(COO^-)_{asym}$ 1482, symmetric carboxylic $\nu(COO^-)_{sym}$ 1390, $\nu(H_2O)$ stretching bands of coordinated water 933 and 842, $\nu(M-O)$ stretching bands of coordinated water 533, metal–nitrogen bond $\nu(M-N)$ 470. 1H NMR (300 MHz, DMSO- d_6 , δ , ppm): 7.27–8.00 (m, 21H, Ar H), 5.74 (s, 2H, OH carboxylate). ^{13}C NMR (300 MHz, DMSO- d_6 , δ , ppm): 161.5 (C1 and C6; pyridine ring), 114.3 (C2 and C4; pyridine ring), 136.6 (C3; pyridine ring), 174.2 (C5; C=N azomethine), 167.4 (C14; COOH), 136.3 (C6; Ar), 129.1 (C7, C11; Ar), 128.5 (C8, C10; Ar), 130.7 (C9; Ar), 137.8 (C12; benzoic), 131.5 (C13; benzoic), 128.2 (C15; benzoic), 130.4 (C16; benzoic), 133.7 (C17; benzoic), 125.7 (C18; benzoic). λ_{max} (nm): 217 and 245 $\pi-\pi^*$, 332 $n-\pi^*$.

CdH₂L

Yield 85%; yellowish green solid, m.p. 140°C. Anal. Calcd for $Cd(C_{33}H_{29}Cl_2N_3O_7)$ (%): C, 51.97; H, 3.81; N, 5.51; Cd, 14.70. Found (%): C, 52.21; H, 4.13; N, 5.55; Cd, 14.57. FT-IR (cm^{-1}): hydroxyl $\nu(OH)$ 3439, azomethine $\nu(C=N)$ 1604, asymmetric carboxylic $\nu(COO^-)_{asym}$ 1545, symmetric carboxylic $\nu(COO^-)_{sym}$ 1384, $\nu(H_2O)$ stretching bands of coordinated water 931 and 844, $\nu(M-O)$ stretching bands of coordinated water 561, metal–nitrogen bond $\nu(M-N)$ 489. 1H NMR (300 MHz, DMSO- d_6 , δ , ppm): 7.17–8.00 (m, 21H, Ar H), 5.70 (s, 2H, OH carboxylate). λ_{max} (nm): 240 $\pi-\pi^*$, 334 $n-\pi^*$.

Spectrophotometric studies

The absorption spectra were recorded for 1×10^{-4} M solutions of the Schiff base ligand and its metal complexes in DMF, except for Cu(II) and Fe(III) complexes that had a concentration of 5×10^{-5} M. The spectra were scanned within the wavelength range from 200 to 700 nm.

Pharmacology

Antimicrobial activity

A filter paper disc (5 mm) was transferred into each of 250 mL flasks containing 20 mL of working volume of test solution (100 mg mL^{-1}). All flasks were autoclaved for 20 min at 121°C . LB agar media surfaces were inoculated with four investigated bacteria (Gram-positive bacteria: *Bacillus subtilis* and *Staphylococcus aureus*; Gram-negative bacteria: *Neisseria gonorrhoeae* and *Escherichia coli*) and one strain of fungi (*Candida albicans*) using the diffusion agar technique.^[13–15] They were then transferred to saturated discs with a test solution in the centre of Petri dishes (agar plates). All the compounds were placed at four equidistant places at a distance of 2 cm from the centre of the inoculated Petri dishes. DMSO served as control. Finally, all these Petri dishes were incubated at 25°C for 48 h where clear or inhibition zones were detected around each disc. Control flask of the experiment was designed to perform the experiment under the same condition described previously for each microorganism but with DMF solution only and by subtracting the diameter of the inhibition zone resulting from DMF from that obtained in each case, so antibacterial activity could be calculated.^[16,17] Amikacin and ketokonazole were used as reference compounds for antibacterial and antifungal activities, respectively. All experiments were performed as triplicate and data plotted were the mean values.

Anticancer activity

Potential cytotoxicity of the compounds was tested using the method of Skehan and Storeng.^[16,18] Cells were plated in a 96-multiwell plate (104 cells per well) for 24 h before treatment with the compounds to allow attachment of cells to the wall of the plate. Various concentrations of the compounds under investigation (0, 5, 12.5, 25, 50 and $100 \mu\text{g mL}^{-1}$) were added and cell monolayer triplicate wells were prepared for each individual dose. The monolayer cells were incubated with the compounds for 48 h at 37°C and in 5% CO_2 atmosphere. After 48 h, cells were fixed, washed and stained with SRB. Excess stain was washed with acetic acid and attached stain was recovered with Tris–EDTA buffer. The OD of each well was measured spectrophotometrically at 564 nm with an ELIZA microplate reader and the mean background absorbance was automatically subtracted, and mean values of each drug concentration were calculated. The relation between surviving fraction and drug concentration was plotted to get the survival curve of breast tumour cell line for each compound.

The percentage of cell survival was calculated as follows:

$$\text{Survival fraction} = \frac{\text{OD (treated cells)}}{\text{OD (control cells)}}$$

The IC_{50} values (the concentrations of the Schiff base ligand or its complexes required to produce 50% inhibition of cell growth) were calculated. The experiment was repeated three times for MCF7 cell line.

Results and discussion

Characterization of Schiff base ligand

The symmetric Schiff base ligand was prepared by stirring an appropriate amount of *o*-benzoylbenzoic acid with the corresponding 2,6-diaminopyridine in ethanol. The new Schiff base ligand formed was characterized with respect to its composition using elemental and spectral analyses.

Elemental Analysis

The synthesized Schiff base ligand, namely 2,2'-((1Z,1'Z)-(pyridine-2,6-diylbis(azanylylidene))-bis(phenylmethanylylidene))dibenzoic acid, is a yellowish green solid and stable at room temperature. It is soluble in ethanol, DMF and DMSO. The results obtained are in good agreement with those calculated for the suggested formula. The structure of the symmetric Schiff base ligand under study is shown in Fig. 1.

Mass Spectrum

The mass spectrum of the Schiff base ligand was recorded and the obtained molecular ion (m/z) peaks confirm its proposed formula and geometry. The ligand shows a peak at $m/z = 526$ amu corresponding to the $[\text{C}_{33}\text{H}_{23}\text{N}_3\text{O}_4]^+$ ion. It also showed a series of peaks at $m/z = 499, 404, 372, 316, 233, 196, 105$ and 56 corresponding to various fragments. The intensity of these peaks gives an idea of the stabilities of fragments.

FT-IR Spectrum

The FT-IR spectrum of 2,6-diaminopyridine shows a pair of medium intensity bands present at $3200\text{--}3400 \text{ cm}^{-1}$ which correspond to $\nu(\text{NH}_2)$ stretching vibration. These bands are absent in the spectrum of the Schiff base ligand. Also, no strong absorption band is observed at 1735 cm^{-1} indicating the absence of $\nu(\text{C}=\text{O})$ group of *o*-benzoylbenzoic acid. This indicates that the condensation of carbonyl groups of *o*-benzoylbenzoic acid and amino groups of 2,6-diaminopyridine has taken place.^[19,20] A new band for the azomethine $\nu(\text{C}=\text{N})$ stretching vibration was recorded due to this condensation reaction at 1596 cm^{-1} .^[21,22]

^1H NMR Spectrum

In the ^1H NMR spectrum of H_2L , the aromatic ring protons are observed as a multiplet, in the range 7.17–8.00 ppm.^[23] A peak at 5.68 ppm is attributed to proton of the carboxylic acid group.^[24] This small shift can be attributed to the intramolecular hydrogen bonding with the solvent.

Compositions and structures of metal complexes

Elemental analyses

Metal complexes were prepared by the reaction of metal ions with Schiff base ligand at a metal-to-ligand ratio of 1:1. The Schiff base ligand and its metal complexes are stable at room temperature.

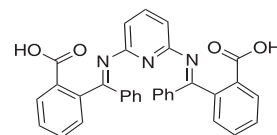


Figure 1. Structure of macrocyclic Schiff base ligand (H_2L).

The ligand and its metal complexes are commonly soluble in DMF and DMSO. The analytical data are compatible with the proposed stoichiometry of the complexes.^[25]

Molar conductance measurements

The molar conductance values of the complexes were measured at room temperature. These values show that Cu(II), Zn(II) and Cd(II) complexes have no conductance and they are considered as non-electrolytes. Cr(III), Mn(II), Co(II) and Ni(II) complexes have molar conductivity values of 77, 75, 60 and 61 $\Omega^{-1} \text{ mol}^{-1} \text{ cm}^2$, respectively. These data suggest that these complexes are ionic in nature and they are 1:1 electrolytes. The Fe(III) complex has a molar conductivity value of 111 $\Omega^{-1} \text{ mol}^{-1} \text{ cm}^2$, which suggests that this complex is ionic in nature and it is a 1:2 electrolyte.^[26]

FT-IR spectral studies and mode of bonding

The FT-IR spectral data for the Schiff base ligand and its complexes are listed in Table S1 of the supporting information. The FT-IR spectra of the complexes were compared with that of the free ligand in order to determine the involvement of coordination sites in chelation. The FT-IR spectra of the metal complexes exhibit a broad band around 3318–3450 cm^{-1} which is assigned to $\nu(\text{OH})$ of coordinated water molecules associated with the complex, while it appears in the ligand spectrum at 3455 cm^{-1} . This band may be assigned to the presence of hydrogen bonded O-H.^[27,28]

The FT-IR spectrum of the ligand shows a characteristic absorption band at 1596 cm^{-1} corresponding to $\nu(\text{C}=\text{N})$ of azomethine group. For all the metal complexes, the $\nu(\text{C}=\text{N})$ band of the azomethine is shifted to 1578–1615 cm^{-1} , while it is absent in case of the Cr(III) complex, suggesting coordination of azomethine nitrogen to metal ions.^[29]

The $\nu_{\text{asym}}(\text{COO}^-)$ and $\nu_{\text{sym}}(\text{COO}^-)$ stretching vibrations are observed at 1540 and 1380 cm^{-1} in the FT-IR spectrum of H_2L .^[30] These bands are present in the range 1466–1545 and 1383–1410 cm^{-1} in the spectra of the metal complexes.^[31] This shift can be attributed to intramolecular hydrogen bonding. The coordinating water in the complexes is characterized by the appearance of two bands at 931–993 and 837–896 cm^{-1} .^[32]

The coordination of the azomethine nitrogen is supported by the appearance of a new metal–ligand weak band at 458–489 cm^{-1} due to $\nu(\text{M}-\text{N})$.^[33,34]

Additional support for the formation of the complexes is provided by presence of weak-intensity bands at 519–583 cm^{-1} which are attributed to the formation of M–O of coordinated water in the complexes.^[22]

¹H NMR spectral studies

Proof of the type of bonding type of H_2L with the metal ions was also confirmed by recording their ¹H NMR spectra in DMSO-*d*₆ and in the deuterated solvent.^[33–35] In the spectrum of H_2L a singlet peak appears at 5.68 ppm (s, 2H, COOH carboxylic). This peak is found in the spectra of Zn(II) and Cd(II) complexes at 5.74 and 5.70 ppm, respectively, indicating that the carboxylic groups play no important part in coordination.^[36] This small shift can be attributed to the intramolecular hydrogen bonding with the solvent.

The ¹H NMR spectrum of the ligand reveals signals at 7.17–8.00 ppm (m, 21H, Ar-H), while for Zn(II) and Cd(II) complexes the signals are at 7.27–8.00 and 7.17–8.01 ppm (m, 21H, Ar-H), respectively, which can be assigned to the aromatic protons.^[37]

Mass spectral studies

Mass spectroscopy has been increasingly used as a powerful structural characterization technique in coordination chemistry. The spectra of the Mn(II) and Ni(II) complexes show molecular ion peaks at $m/z = 701.22$ and 705.71 amu, respectively, which are equivalent to their molecular weights of 705 and 709 amu, respectively. The molecular ion peaks are in good agreement with the suggested molecular formulae indicated from elemental and TG analyses.

UV-visible absorption studies

The electronic spectra of the Schiff base ligand and its complexes were recorded in DMF solvent within the wavelength range 200–700 nm. In the UV-visible spectrum of the Schiff base ligand, two absorption bands are observed at 217 and 246 nm which may be assigned to $\pi-\pi^*$ transitions of the aromatic rings.^[38,39] Also, the absorption band at 333 nm may be assigned to $n-\pi^*$ transition of the azomethine or carboxylate groups. Due to the coordination of azomethine nitrogen to the metal ions, this band is seen in the absorption spectra of all complexes at 317–335 nm. Also, the band due to $\pi-\pi^*$ transition is observed at 213–245 nm in the spectra of all metal complexes.^[40]

Electronic spectra and magnetic moment measurements

The Cr(III) chelate which is six-coordinated with octahedral symmetry shows four spin-allowed bands at 17 249, 20 014, 21 457 and 22 059 cm^{-1} . These bands may be assigned to ${}^4\text{A}_{2g}(\text{F}) \rightarrow {}^4\text{T}_{2g}(\text{F})$, ${}^4\text{A}_{2g}(\text{F}) \rightarrow {}^4\text{T}_{2g}(\text{F})$, ${}^4\text{A}_{2g}(\text{F}) \rightarrow {}^4\text{T}_{1g}(\text{F})$ and ${}^4\text{A}_{2g}(\text{F}) \rightarrow {}^4\text{T}_{1g}(\text{P})$ transitions indicating the octahedral geometry of the complex. The magnetic moment value of 3.82 BM indicates the presence of Cr(III) complex in an octahedral structure.^[26]

The diffuse reflectance spectrum of the Mn(II) complex shows three bands at 15 560, 21 478 and 27 876 cm^{-1} assignable to ${}^4\text{T}_{1g} \rightarrow {}^6\text{A}_{1g}$, ${}^4\text{T}_{2g}(\text{G}) \rightarrow {}^6\text{A}_{1g}$ and ${}^4\text{T}_{1g}(\text{D}) \rightarrow {}^6\text{A}_{1g}$ transitions, respectively.^[25] The magnetic moment value of 5.44 BM indicates the presence of Mn(II) complex in an octahedral structure.

The diffuse reflectance spectrum of the Fe(III) chelate exhibits a band at 21 357 cm^{-1} , which may be assigned to the ${}^6\text{A}_{1g} \rightarrow \text{T}_{2g}(\text{G})$ transition of octahedral geometry of the complex.^[41] The ${}^6\text{A}_{1g} \rightarrow {}^5\text{T}_{1g}$ transition appears to be split into two bands at 17 135 and 12 970 cm^{-1} . The observed magnetic moment of the Fe(III) complex is 5.38 BM. Thus, the complex formed has octahedral geometry involving d^2sp^3 hybridization in Fe(III) ion.^[42] The spectrum also shows a band at 24 805 cm^{-1} which may be attributed to ligand to metal charge transfer.

The Cu(II) complex shows broad bands at 12 466, 15 750 and 19 945 cm^{-1} . These bands are generally completely consistent with a five-coordinate geometry for Cu(II) complexes.^[43–45] The spectrum also shows a band at 30 452 cm^{-1} which may be assigned to ligand to Cu charge transfer band. The magnetic moment value of 1.78 BM is indicative of a trigonal bipyramidal structure.^[43,44,46,47]

The diffuse reflectance spectrum of the Co(II) complex shows that the complex has five-coordinated geometry,^[47] where three bands are observed at 13 050, 15 886 and 17 594 cm^{-1} . The fourth band at 21 378 cm^{-1} is attributed to the charge transfer band. The value of the magnetic moment of the complex is 5.0 BM, which is low compared with those observed for tetrahedral or octahedral complexes, and which supports five-coordinate geometry.^[47]

The reflectance spectrum of the Ni(II) complex shows three bands at 13 670, 17 245 and 21 444 cm^{-1} . The positions of these spectral bands are completely consistent with those predicted for a five-coordinate Ni(II) complex.^[48] Those bands can be assigned,

respectively,^[48] to ${}^3B_1 \rightarrow {}^3E$, ${}^3B_1 \rightarrow {}^3A_2$ and ${}^3B_1 \rightarrow {}^3E$ transitions assuming the effective symmetry to be C_{4v} . The band at $27\,379\text{ cm}^{-1}$ may be assigned to ligand to metal charge transfer band.^[47] The low magnetic moment value (3.21 BM) may support the five-coordinate geometry.

The Zn(II) and Cd(II) complexes are diamagnetic. According to their empirical formulae, the Zn(II) and Cd(II) complexes are suggested to have trigonal bipyramidal geometry.^[26]

Powder XRD studies

Powder diffraction is a technique that uses X-ray, neutron or electron diffraction on powder or microcrystalline samples for structural characterization of materials. It throws light only on the fact that each solid represents a definite compound of a definite structure which is not contaminated with starting materials. The identification of the complexes was performed using a known standard method.^[26] The results suggest that the synthesized Fe(III), Co(II), Ni(II), Cu(II), Zn(II) and Cd(II) complexes are amorphous. In contrast, the XRD spectra of H_2L and its Cr(III) and Mn(II) complexes indicate a crystalline character.^[49,50]

The average crystallite size (ξ) can be calculated from the XRD pattern according to the Debye–Scherrer equation:^[51,52]

$$\xi = \frac{K\lambda}{\beta_{1/2} \cos\theta} \quad (1)$$

The equation uses the reference peak width at angle θ , where λ is the wavelength of the X-rays (1.542475 \AA), K is a constant taken as 0.95 for organic compounds^[51] and $\beta_{1/2}$ is the width at half maximum of the reference diffraction peak measured in radians. The dislocation density, δ , is the number of dislocation lines per unit area of the crystal. The value of δ is related to the average particle diameter (ξ) by the relation^[53,54]

$$\delta = \frac{1}{\xi^2} \quad (2)$$

The value of ξ is calculated and found to be 0.146 nm and the value of δ is 46.91 nm^{-2} for both H_2L and the Mn(II) complex, while the value of ξ is 0.1455 nm and value of δ is 47.24 nm^{-2} for the Cr(III) complex.

Thermal analysis studies (TG and DTG)

The thermal properties of ligand and its complexes were characterized on the basis of TG and DTG methods within a temperature range from room temperature to 1000°C . These methods are used to get information about the thermal stability of these new complexes, to decide whether the water molecules (if present) are inside or outside the inner coordination sphere of the central metal ion and to suggest a general scheme for thermal decomposition of these chelates. The temperature intervals and the percentage of loss of masses are listed in Table S2 of the supporting information.

The Schiff base ligand with molecular formula $[C_{33}H_{23}N_3O_4]$ is thermally decomposed in five successive decomposition steps. The first and second steps with estimated mass loss of 36.54% (calculated mass loss = 37.14%) within the temperature range $30\text{--}290^\circ\text{C}$ may be attributed to the loss of $C_{13}H_7O_2$ molecule. The DTG curve gives maximum peak temperatures at 66 and 256°C . The third step occurs within the range $290\text{--}355^\circ\text{C}$ with an estimated mass loss of 12.11% (calculated mass loss = 12.00%) which

corresponds to the loss of $C_2H_7O_2$ fragment. The DTG curve gives a peak at 325°C . The final two steps occur within the range $355\text{--}1000^\circ\text{C}$ with estimated mass loss of 50.95% (calculated mass loss = 50.86%) which corresponds to the loss of $C_{18}H_9N_3$ fragment.

The TG curve for the $[Cr(H_2L)(H_2O)_2Cl_2]Cl \cdot 2H_2O$ complex shows three weight loss events. The first step of decomposition occurs within the range $30\text{--}140^\circ\text{C}$, with a maximum at 124°C and corresponds to the loss of two water molecules of hydration with estimated mass loss of 5.59% (calculated mass loss = 4.77%). The second step of decomposition occurs in the range $140\text{--}410^\circ\text{C}$ with maximum temperature at 281°C and corresponds to the loss of two coordinated water molecules, ${}^3/2Cl_2$ gas and $C_{10}H_{10}$ molecule with estimated mass loss of 35.76% (calculated mass loss = 36.07%). The final three steps occur within the range $410\text{--}1000^\circ\text{C}$ with three maxima at 481 , 752 and 894°C which correspond to loss of $C_{23}H_{13}N_3O_3$ fragment with estimated mass loss of 49.97% (calculated mass loss = 50.17%) leaving behind ${}^1/2Cr_2O_3$ as the product of decomposition. The overall weight loss amounts to 91.32% (calculated mass loss = 91.01%).

The $[Mn(H_2L)(H_2O)_3Cl]Cl \cdot H_2O$ complex loses water upon heating in the first step of decomposition within the range $30\text{--}120^\circ\text{C}$ with maximum at 90°C with estimated mass loss of 2.81% (calculated mass loss = 2.49%). The second step can be attributed to the loss of $3H_2O$ and $2CN$ gas within the range $120\text{--}310^\circ\text{C}$ with maximum at 242°C with estimated mass loss of 14.90% (calculated mass loss = 14.66%). The last two steps are attributed to loss of $C_{20}H_{23}N_3O_3$ within the range $310\text{--}1000^\circ\text{C}$ with two maxima at 443 and 792°C with estimated mass loss of 54.34% (calculated mass loss = 54.77%), leaving MnO contaminated with carbon as residue of decomposition. The overall weight loss amounts to 72.05% (calculated 71.92%).

The $[Fe(H_2L)(H_2O)_3Cl]Cl_2 \cdot H_2O$ complex is thermally decomposed in six steps within the range $30\text{--}1000^\circ\text{C}$. The first decomposition step with an estimated mass loss of 3.59% (calculated 2.37%) occurs within the range $30\text{--}140^\circ\text{C}$ with maximum at 63°C . This step may be attributed to the liberation of the hydrated water molecule. The second and third decomposition steps are observed within the range $140\text{--}440^\circ\text{C}$ with two maxima at 250 and 432°C . The estimated mass loss of 16.98% (calculated 17.31%) is reasonably accounted for by the removal of $3H_2O$, ${}^1/2Cl_2$ and C_3H_6 molecules in two steps. The last three steps with estimated mass loss of 45.24% (calculated 46.08%) occur within the range $440\text{--}1000^\circ\text{C}$ with three maxima at 594 , 912 and 984°C and correspond to loss of Cl_2 gas and $C_{15}H_{15}N_3O_{2.5}$ fragment leaving ${}^1/2Fe_2O_3$ contaminated with carbon as residue. The overall weight loss amounts to 65.81% (calculated 65.76%).

The DTG curve of $[Co(H_2L)(H_2O)_2Cl]Cl \cdot H_2O$ shows a peak at 137°C in the range $50\text{--}160^\circ\text{C}$ which is due to weight loss of 3.77% (calculated weight loss = 2.54%) corresponding to the elimination of hydrated water molecule. The second and third steps of the thermal decomposition, which occur in the range $160\text{--}525^\circ\text{C}$ with two maxima at 233 and 439°C , are assigned to the loss of Cl_2 gas, $2H_2O$ and $C_5H_{12}O$ fragment (found 26.68% ; calculated 27.50%). The fourth and fifth steps of the thermal decomposition, which occur in the range $525\text{--}940^\circ\text{C}$, are assigned to the loss of $C_{28}H_{11}N_3O_2$ (found 58.08% ; calculated 59.38%). At the end of the thermogram, the metal oxide CoO is the residue, with total weight loss amounting to 88.53% (calculated = 89.42%).

The $[Ni(H_2L)(H_2O)_2Cl]Cl \cdot H_2O$ complex gives a decomposition pattern starting at 30°C and finishing at 785°C with three stages. The first stage is one step within the range $30\text{--}105^\circ\text{C}$ with maximum at 85°C , representing the loss of H_2O (hydrated) and ${}^1/2Cl_2$ with a

mass loss of 6.21% (calculated 7.55%). The second stage is also one step representing the loss of $\frac{1}{2}\text{Cl}_2$, $2\text{H}_2\text{O}$ and CN with a mass loss of 13.21% (calculated 13.75%) within the range 105–235°C with maximum at 140°C. The final stage is four steps representing the loss of $\text{C}_{32}\text{H}_{23}\text{N}_2\text{O}_3$ with a mass loss of 69.28% (calculated 68.12%) within the range 235–785°C. At the end of the thermogram, the metal oxide NiO is the residue, which is in good agreement with the calculated metal content obtained and the results of elemental analyses.

The complex $[\text{Cu}(\text{H}_2\text{L})(\text{H}_2\text{O})\text{Cl}_2]\cdot 2\text{H}_2\text{O}$ is thermally decomposed in five successive decomposition steps. The first estimated mass loss of 4.26% (calculated mass loss = 5.05%) within the range 25–190°C may be attributed to the loss of two hydrated water molecules. The DTG curve gives an exothermic peak at 79°C (the maximum peak temperature). The second step occurs within the range 190–380°C with an estimated mass loss of 40.12% (calculated mass loss = 39.38%) which corresponds to the loss of H_2O , Cl_2 and $\text{C}_{13}\text{H}_8\text{N}_2$ fragment. The DTG curve gives an exothermic peak at 267°C. The final three steps occur within the temperature range 380–950 °C with the estimated mass loss 44.68% (calculated mass loss = 44.43%) which corresponds to the loss of $\text{C}_{20}\text{H}_{15}\text{NO}_3$ fragment. The DTG curve gives three exothermic peaks at 426, 492 and 742°C, leaving metal oxide CuO as residue. Total estimated mass loss is 89.06% (calculated mass loss = 88.86%).

The $[\text{Zn}(\text{H}_2\text{L})(\text{H}_2\text{O})\text{Cl}_2]\cdot 2\text{H}_2\text{O}$ chelate exhibits four decomposition steps. The first and second steps in the range 30–330°C with two maxima at 81 and 238°C represent losses of $3\text{H}_2\text{O}$ and CN molecule with estimated mass loss of 10.79% (calculated 11.19%). The third step at 330–510°C with maximum at 433°C corresponds to loss of Cl_2 molecule with estimated mass loss of 10.79% (calculated 9.93%). The fourth step within the range 510–910°C with maximum at 674°C corresponds to elimination of $\text{C}_{30}\text{H}_{23}\text{N}_2\text{O}_3$ with a mass loss 63.98% (calculated 64.20%), leaving ZnO and 2C as residues. The overall weight loss amounts to 85.56% (calculated 85.32%).

The $[\text{Cd}(\text{H}_2\text{L})(\text{H}_2\text{O})\text{Cl}_2]\cdot 2\text{H}_2\text{O}$ complex decomposes within the range 75–1000°C with four steps as follows. The first step is within the range 75–205°C with maximum at 93°C, representing the loss $2\text{H}_2\text{O}$ with a found mass loss of 4.03% (calculated 4.72%). The second step represents the loss of H_2O , Cl_2 and C_4H_8 with a mass loss of 19.62% (calculated 19.03%) within the range 205–295°C. The other two steps represent elimination of $\text{C}_{29}\text{H}_{15}\text{N}_3\text{O}_3$ with a mass loss of 60.84% (calculated 59.45%) within the range 295–1000°C. At the end of the thermogram, the metal oxide CdO is the residue. Total estimated mass loss is 84.49% (calculated 83.20%).

Kinetics

The kinetic thermodynamic parameters such as energy of activation (E^*), enthalpy (ΔH^*), entropy (ΔS^*) and free energy change (Gibbs free energy) of decomposition (ΔG^*) are evaluated graphically by employing the Coats–Redfern^[45] and Horowitz–Metzger^[55] equations. The data are summarized in Table S3 of the supporting information.

Coats–Redfern equation

The Coats–Redfern equation, which is a typical integral method, can be represented as:

$$\int_0^\alpha \frac{d\alpha}{(1-\alpha)^n} = \frac{A}{\alpha} \int_{T_1}^{T_2} \exp\left(\frac{-E^*}{RT}\right) dt$$

For convenience of integration, the lower limit T_1 is usually taken as zero. This equation on integration gives

$$\ln\left[\frac{-\ln(1-\alpha)}{T^2}\right] = \frac{-E^*}{RT} + \ln\left(\frac{AR}{\phi E^*}\right)$$

If a plot of the left-hand side against $1/T$ is drawn, E^* (the energy of activation in kJ mol^{-1}) is calculated from the slope and A (s^{-1}) from the intercept. The entropy of activation ΔS^* (in $\text{J K}^{-1} \text{mol}^{-1}$) is calculated using the equation

$$\Delta S^* + R \ln\left(\frac{Ah}{K_B T_s}\right)$$

where K_B is the Boltzmann constant, h is the Planck constant and T_s is the DTG peak temperature.

Horowitz–Metzger equation

The Horowitz–Metzger equation is illustrative of the approximation methods. Those authors derived the relation

$$\log\left[1 - \frac{(1-\alpha)^{1-n}}{1-n}\right] = \frac{E^* \theta}{2.303RT_s^2} \quad \text{for } n \neq 1$$

When $n = 1$, the left-hand side would be $\log[-\log(1-\alpha)]$. For a first-order kinetic process the Horowitz–Metzger equation may be written in the form

$$\log\left[\log\left(\frac{w_\alpha}{w_\gamma}\right)\right] = \frac{E^* \theta}{2.303RT_s^2} - \log 2.303$$

where $\theta = T - T_s$, $w_\gamma = w_\alpha - w$, w_α is mass loss at the completion of the reaction and w is mass loss up to time t . A plot of $\log[\log(w_\alpha/w_\gamma)]$ versus θ is found to be linear, from the slope of which E^* is calculated. The pre-exponential factor, A , is calculated from the equation

$$\frac{E^*}{RT_s^2} = \frac{A}{\phi \exp(-E^*/RT_s)}$$

The entropy of activation, ΔS^* , enthalpy of activation, ΔH^* and Gibbs free energy, ΔG^* , are calculated using the following equations:

$$\Delta H^* = E^* - RT$$

$$\Delta G^* = \Delta H^* - T\Delta S^*$$

The activation energies of decomposition are found to be in the range 12.50–130.8 kJ mol^{-1} . The greater positive values of E^* indicate that these processes involve translational, vibrational, rotational states and changes in mechanical potential energy for the complexes. The high values of the activation energies show the thermal stability of the complexes. The entropy of activation is found to have negative values for all metal complexes which indicate that decomposition reactions proceed with a lower rate than normal ones. Also, according to the kinetic data obtained, all of the complexes have negative entropy, which indicates that activated complexes have more ordered systems than reactants.^[56–58]

Structural interpretation

On the basis of the various physicochemical and spectral data presented and discussed above, the structures of the Cr(III), Mn(II), Fe(III), Co(II), Ni(II), Cu(II), Zn(II) and Cd(II) complexes are shown in Fig. 2.

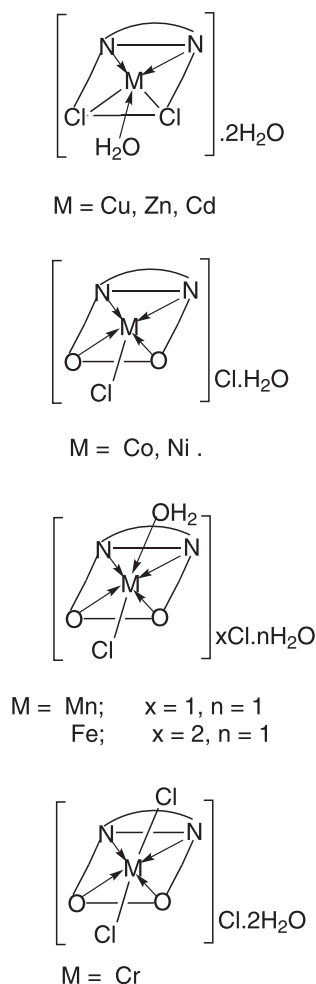


Figure 2. Structures of metal complexes.

Antimicrobial activity

The principal aim of any antimicrobial compound is to inhibit the causal microbes without any side effects on patients.^[59]

The Schiff base ligand and its metal complexes were tested against four different bacteria species: *S. aureus*, *B. subtilis*, *E. coli* and *N. gonorrhoeae*. Also, they were screened against *C. albicans* fungal strain.^[60] The biological activities of the ligand and its complexes were compared with those of the standards amikacin as antibacterial agent and ketokonazole as antifungal agent.^[26]

The experimental data are presented in Table S4 of the supporting information and compared with standards as shown in Fig. 3. These data show that the metal complexes are more potent in inhibiting the growth of microorganisms than the Schiff base ligand, except the Fe(III) complex which has no activity against *B. subtilis* and *E. coli* and the Cd(II) complex which also has no activity against *S. aureus*. It is determined that the synthesized Mn(II) complex may have the same antibacterial activity as that of the parent Schiff base ligand but higher against *S. aureus*.^[61,62]

The bacterial growth inhibitory capacity of the ligand and its complexes follows the order Zn(II) = Cd(II) > Cu(II) > Cr(III) > Co(II) = Ni(II) > H₂L = Mn(II) > amikacin > Fe(III) (for *B. subtilis*); Co(II) > Mn(II) = Cu(II) > Zn(II) > Cr(III) = Fe(III) > Ni(II) > H₂L > amikacin > Cd(II) (for *S. aureus*); Zn(II) > Co(II) > Cd(II) > Cu(II) > Cr(III) = Ni(II) > Mn(II) > H₂L > amikacin > Fe(III)

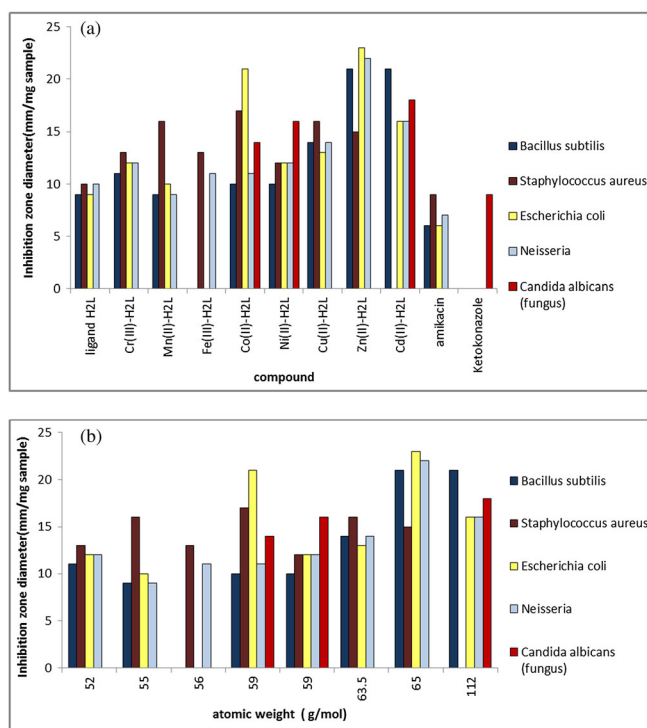


Figure 3. (a) Biological activity of Schiff base ligand (H₂L) and its metal complexes and (b) variation of biological activity with atomic weight of metal ion.

(for *E. coli*); Zn(II) > Cd(II) > Cu(II) > Cr(III) = Ni(II) > Fe(III) = Co(II) > H₂L > Mn(II) > amikacin (for *N. gonorrhoeae*).^[16]

It is obvious that the biological activities of the metal complexes are more than that of the parent Schiff base ligand which means that the complexes can have better action than the parent ligand. The biological activities of the Schiff base ligand and its complexes are higher than that of amikacin standard.

By comparing the results of antifungal activity of the Schiff base ligand and its complexes with the standard, it is obvious that they have no activity against *C. albicans* strain, except Co(II), Ni(II) and Cd(II) complexes which have high activity. The variation in the activity of the metal complexes against different organisms depends on the impermeability of the microorganism cells or on differences in ribosome of microbial cells.^[63]

The size of the inhibition zone depends upon the culture medium, incubation conditions, rate of diffusion and concentration of antibacterial agent. The activities of all the tested complexes may be explained on the basis of chelation theory where chelation reduces the polarity of the metal atom mainly because of partial sharing of its positive charge with the donor groups and possible p-electron delocalization within the whole chelate ring. Also, chelation increases the lipophilic nature of the central atom which subsequently favours its permeation through the lipid layer of cell membranes.^[64]

The importance of this study lies in the fact that these complexes could be applied in the treatment of some common diseases caused by *E. coli*, e.g. septicaemia, gastroenteritis, urinary tract infections and hospital-acquired infections.^[65]

Anticancer activity

The *in vitro* cytotoxicity of H₂L and its metal complexes on human cell line MCF-7 was studied. The results of the IC₅₀ values of the

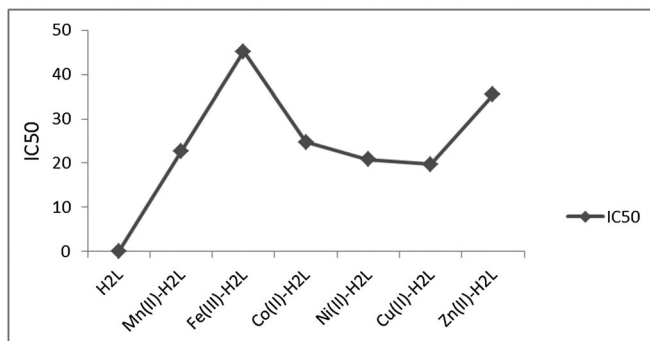


Figure 4. IC₅₀ values of Schiff base ligand (H₂L) and its metal complexes.

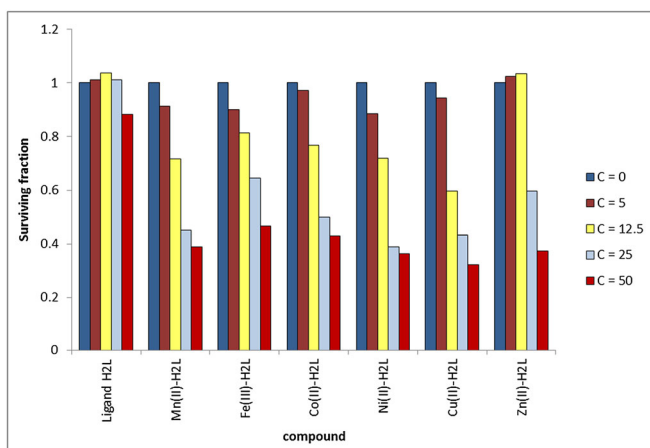


Figure 5. Anticancer activity of Schiff base ligand (H₂L) and its metal complexes.

complexes are summarized in Table S5 of the supporting information, and shown in Fig. 4.^[66,67] The pattern of activity can be determined using various concentrations of the Schiff base ligand or its metal complexes (Fig. 5). The majority of the complexes are active against the MCF-7 cell line while H₂L has no activity. The IC₅₀ values of the metal complexes range from 19.7 to 45.2 μg μL⁻¹, and the order of IC₅₀ for this cancer cell line can be arranged as follows: standard < Cu(II) < Ni(II) < Mn(II) < Co(II) < Zn(II) < Fe(III).^[25]

Conclusions

In summary, the work reported involved the synthesis and spectroscopic characterization of a series of Cr(III), Mn(II), Fe(III), Co(II), Ni(II), Cu(II), Zn(II) and Cd(II) complexes with a new Schiff base ligand prepared by condensation of 2,6-diaminopyridine with *o*-benzoylbenzoic acid. The complexes were characterized using various physicochemical techniques. The Schiff base ligand acts as a bidentate (NN) ligand through the two azomethine nitrogen atoms and all complexes show trigonal bipyramidal geometry, except Cr(III), Mn(II) and Fe(III) complexes which have octahedral geometry. Their molar conductance values confirm that Cu(II), Zn(II) and Cd(II) complexes are non-electrolytes, while the Cr(III), Mn(II), Co(II) and Ni(II) complexes are 1:1 electrolytes and the Fe(III) complex is a 1:2 electrolyte. From elemental analysis, the complexes have composition of the MH₂L type with general formulae [M(H₂L)(H₂O)₃Cl] \cdot *n*H₂O (M = Mn(II), *x* = *n* = 1; Fe(III), *x* = 2, *n* = 1), [M(H₂L)(H₂O)₂Cl] \cdot *n*H₂O (M = Co(II) and Ni(II)), [M(H₂L)(H₂O)Cl₂] \cdot 2H₂O

(M = Cu(II), Zn(II) and Cd(II)) and [M(H₂L)(H₂O)₂Cl₂] \cdot 2H₂O (M = Cr(III)). XRD spectra show that the Fe(III), Co(II), Ni(II), Cu(II), Zn(II) and Cd(II) complexes are amorphous. On the other hand, the ligand and its Cr(III) and Mn(II) complexes have a crystalline character. The ligand and metal complexes are found to possess appreciable antibacterial activity, except the Fe(III) complex which has no activity against *B. subtilis* and *E. coli* and the Cd(II) complex which also has no activity against *S. aureus*. The Co(II), Ni(II) and Cd(II) complexes have high antifungal activity. In addition, the cytotoxicity of the Cu(II) complex indicates a higher anticancer activity than the others with IC₅₀ of 19.7 μg mL⁻¹, which might become a good anticancer agent in clinical trials or biological agents.

References

- [1] A. M. A. Alaghaz, M. E. Zayed, S. A. Alharbi, R. A. A. Ammar, *J. Mol. Struct.* **2015**, *1087*, 60–7.
- [2] H. Keypour, A. Shooshtari, M. Rezaeivala, F. O. Kup, H. A. Rudbari, *Polyhedron* **2015**, *97*, 75–82.
- [3] N. E. Borisova, M. D. Reshetova, Y. A. Ustynyuk, *Chem. Rev.* **2007**, *107*, 46–79.
- [4] Kh. Mohammadi, S. S. Azad, A. Amoozegar, *Spectrochim. Acta A* **2015**, *146*, 221–7.
- [5] K. Dhahagani, S. M. Kumar, G. Chakkaravarthi, K. Anitha, J. Rajesh, A. Ramu, G. Rajagopal, *Spectrochim. Acta A* **2014**, *117*, 87–94.
- [6] Y. M. S. A. Al-Kahraman, H. M. F. Madkour, D. Ali, M. Yasinza, *Molecules* **2010**, *15*, 660–71.
- [7] F. A. Bassyouni, H. A. Tawfik, A. Soliman, M. Abdel Rehim, *Res. Chem. Intermed.* **2012**, *38*, 1291–310.
- [8] M. R. H. Keypour, *Coord. Chem. Rev.* **2014**, *280*, 203–53.
- [9] S. Ilhan, H. Temel, R. Ziyadanogullari, M. Sekerci, *Transition Met. Chem.* **2007**, *32*, 584–90.
- [10] S. Ilhan, H. Temel, I. Yilmaz, M. Sekerci, *Polyhedron* **2007**, *26*, 2795–802.
- [11] S. Ilhan, H. Temel, I. Yilmaz, A. Kilic, *Transition Met. Chem.* **2007**, *32*, 344–9.
- [12] S. Ilhan, H. Temel, I. Yilmaz, M. Sekerci, *Organometal. Chem.* **2007**, *692*, 3855–65.
- [13] M. A. Pfaller, L. Burmeister, M. S. Bartlett, M. G. Rinaldi, *J. Clin. Microbiol.* **1988**, *26*, 1437–41.
- [14] Reference method for broth dilution antifungal susceptibility testing of conidium-forming filamentous fungi: proposed standard M38-A, National Committee for Clinical Laboratory Standards, Wayne, PA, **2002**.
- [15] Method for antifungal disc diffusion susceptibility testing of yeast: proposed guideline M44-P, National Committee for Clinical Laboratory Standards, Wayne, PA, **2003**.
- [16] W. H. Mahmoud, G. G. Mohamed, M. M. I. El-Dessouky, *Spectrochim. Acta A* **2014**, *122*, 598–608.
- [17] I. Sakıyan, E. Lo o lu, S. Arslan, N. Sari, N. Şakıyan, *Biometals* **2004**, *17*, 115–20.
- [18] P. Skehan, R. Storeng, *J. Natl. Cancer Inst.* **1990**, *42*, 1107–12.
- [19] D. P. Singh, V. Malik, K. Kumar, C. Sharma, K. R. Aneja, *Spectrochim. Acta A* **2010**, *76*, 45–9.
- [20] D. P. Singh, R. Kumar, P. Tyagi, *Transition Met. Chem.* **2006**, *31*, 970–3.
- [21] K. K. Abid, A. B. Omar, *Res. Chem. Intermed.* **2015**, *41*, 1715–26.
- [22] B. Shafaatian, Z. Ozbakzaei, B. Notash, S. A. Rezvani, *Spectrochim. Acta A* **2014**, *5*, 248–55.
- [23] S. M. Pradeepa, H. S. B. Naik, B. V. Kumar, K. I. Priyadarsini, A. Barik, S. Jayakumar, *Inorg. Chim. Acta* **2015**, *428*, 138–46.
- [24] S. M. Pradeepa, H. S. B. Naik, B. V. Kumar, K. I. Priyadarsini, A. Barik, M. C. Prabhakara, *Spectrochim. Acta A* **2015**, *15*, 34–42.
- [25] G. G. Mohamed, E. M. Zayed, A. M. M. Hindy, *Spectrochim. Acta A* **2015**, *15*, 76–84.
- [26] W. H. Mahmoud, N. F. Mahmoud, G. G. Mohamed, A. A. El-Bindary, A. Z. El-Sonbati, *J. Mol. Struct.* **2015**, *1086*, 266–75.
- [27] O. A. M. Ali, S. M. El-Medani, D. A. Ahmed, D. A. Nassar, *Spectrochim. Acta A* **2015**, *144*, 99–106.
- [28] I. M. Khan, A. Ahmad, S. Kumar, *J. Mol. Struct.* **2013**, *1035*, 38–45.
- [29] M. Mishra, K. Tiwari, P. Mourya, M. M. Singh, V. P. Singh, *Polyhedron* **2015**, *89*, 29–38.
- [30] S. M. Abdallah, M. A. Zayed, G. G. Mohamed, *J. Arabian Chem.* **2010**, *3*, 103–13.

- [31] A. H. Manikshete, S. K. Sarsamkar, S. A. Deodware, V. N. Kamble, M. R. Asabe, *Inorg. Chem. Commun.* **2011**, *14*, 618–21.
- [32] A. A. Abou-Hussein, W. Linert, *Spectrochim. Acta A* **2015**, *141*, 223–32.
- [33] M. M. Abo-Aly, A. M. Salem, M. A. Sayed, A. A. Abdel Aziz, *Spectrochim. Acta A* **2015**, *136*, 993–1000.
- [34] M. M. Aboaly, M. M. H. Khalil, *Spectrosc. Lett.* **2001**, *34*, 495–504.
- [35] S. Y. Ebrahimipour, I. Sheikhshoae, A. C. Kautz, M. Ameri, H. Pasban, H. A. Rudbari, G. Bruno, C. Janiak, *Polyhedron* **2015**, *93*, 99–105.
- [36] A. A. Abou-Hussein, W. Linert, *Spectrochim. Acta A* **2014**, *117*, 763–71.
- [37] G. G. Mohamed, M. M. Omar, A. A. Ibrahim, *Spectrochim. Acta A* **2010**, *75*, 678–85.
- [38] S. Y. Ebrahimipour, I. Sheikhshoae, J. Castro, W. Haase, M. Mohamadi, S. Foro, M. Sheikhshoae, S. E. Mahani, *Inorg. Chim. Acta* **2015**, *430*, 245–52.
- [39] B. Anupama, M. Sunita, D. S. Leela, B. Ushaiah, C. G. Kumari, *J. Fluoresc.* **2014**, *24*, 1067–76.
- [40] J. D. Chellaian, J. Johnson, *Spectrochim. Acta A* **2014**, *127*, 396–404.
- [41] H. F. Abd El-Halim, F. A. Nour El-Dien, G. G. Mohamed, N. A. Mohamed, *J. Therm. Anal. Calorim.* **2013**, *111*, 173–81.
- [42] E. M. Zayed, E. H. Ismail, G. G. Mohamed, M. M. H. Khalil, A. B. Kamel, *Monatsh. Chem.* **2014**, *145*, 755–65.
- [43] F. A. Cotton, G. Wilkinson, C. A. Murillo, M. Bochmann, *Advanced Inorganic Chemistry*, 6th edition, Wiley, New York, **1999**.
- [44] G. G. Mohamed, Z. M. Zaki, *Synth. React. Inorg. Met.-Org. Chem.* **2004**, *34*, 1497–516.
- [45] A. W. Coats, J. P. Redfern, *Nature* **1964**, *201*, 68–9.
- [46] A. A. Soliman, G. G. Mohamed, *Thermochim. Acta* **2004**, *421*, 151–9.
- [47] G. G. Mohamed, *Spectrochim. Acta A* **2006**, *64*, 188–95.
- [48] A. J. Lavery, M. Schroder, *Acta Crystallogr.* **1996**, *CS2*, 37–9.
- [49] J. R. Anacona, J. L. Rodriguez, J. Camus, *Spectrochim. Acta A* **2014**, *129*, 96–102.
- [50] Z. H. Chohan, H. Pervez, A. Rauf, K. M. Khan, C. T. Supuran, *J. Enzyme Inhib. Med. Chem.* **2004**, *19*, 417–23.
- [51] A. Z. El-Sonbati, M. A. Diab, A. A. El-Bindary, G. G. Mohamed, Sh. M. Morgan, *Inorg. Chim. Acta* **2015**, *430*, 96–107.
- [52] N. A. El-Ghamaz, A. Z. El-Sonbati, M. A. Diab, A. A. El-Bindary, G. G. Mohamed, Sh. M. Morgan, *Spectrochim. Acta A* **2015**, *147*, 200–11.
- [53] S. Velumania, X. Mathew, P. J. Sebastian, Sa. K. Narayandass, D. Mangalaraj, *Solar Energy Mater. Solar Cells* **2003**, *76*, 347–58.
- [54] S. Basavaraja, D. S. Balaji, M. D. Bedre, D. Raghunandan, P. M. P. Swamy, A. Venkatarman, *Bull. Mater. Sci.* **2011**, *34*, 1313–7.
- [55] H. W. Horowitz, G. Metzger, *Anal. Chem.* **1963**, *35*, 1464–8.
- [56] A. A. Frost, R. G. Pearson, *Kinetics and Mechanism*, John Wiley, New York, **1961**.
- [57] S. A. Sadeek, W. H. El-Shwiniy, *J. Mol. Struct.* **2010**, *981*, 130–8.
- [58] W. H. Mahmoud, G. G. Mohamed, M. M. I. El-Dessouky, *J. Mol. Struct.* **2015**, *1082*, 12–22.
- [59] H. F. Abd El-Halim, M. M. Omar, G. G. Mohamed, *Spectrochim. Acta A* **2011**, *78*, 36–44.
- [60] H. F. Abd El-Halim, G. G. Mohamed, *J. Mol. Struct.* **2016**, *1104*, 91–5.
- [61] M. H. Soliman, G. G. Mohamed, *Spectrochim. Acta A* **2013**, *107*, 8–15.
- [62] M. Sahin, N. Kocak, D. Erdenay, U. Arslan, *Spectrochim. Acta A* **2013**, *103*, 400–8.
- [63] E. Ispir, *Dyes Pigments* **2009**, *82*, 13–9.
- [64] A. Caudhary, R. V. Singh, *Phosphorus Sulfur Silicon Relat. Elem.* **2003**, *178*, 603–13.
- [65] M. H. Soliman, G. G. Mohamed, *Spectrochim. Acta A* **2012**, *91*, 11–7.
- [66] P. Tyagi, S. Chandra, B. S. Saraswat, D. Yadav, *Spectrochim. Acta A* **2015**, *145*, 155–64.
- [67] S. M. Lee, K. S. Sim, K. M. Lo, *Inorg. Chim. Acta* **2015**, *429*, 195–208.

Supporting information

Additional supporting information may be found in the online version of this article at the publisher's web site.